

Systematic analysis of structural and magnetic properties of spinel CoB_2O_4 (B=Cr,Mn and Fe) compounds from their electronic structures

Debashish Das, Rajkumar Biswas, and Subhradip Ghosh

Department of Physics, Indian Institute of Technology Guwahati, Guwahati, Assam 781039, India

(Dated: August 11, 2016)

The structural and magnetic properties of spinel compounds CoB_2O_4 (B=Cr,Mn and Fe) are studied using the DFT+U method and generalized gradient approximation (GGA). We concentrate on understanding the trends in the properties of these materials as the B cation changes, in terms of relative strengths of crystal fields and exchange fields through an analysis of their electronic densities of states. We find that the electron-electron correlation plays a significant role in obtaining the correct structural and electronic ground states. Significant structural distortion in $CoMn_2O_4$ and "inverted" sublattice occupancy in $CoFe_2O_4$ affects the magnetic exchange interactions substantially. The trends in the magnetic exchange interactions are analysed in terms of the structural parameters and the features in their electronic structures. We find that the Fe states in $CoFe_2O_4$ are extremely localised, irrespective of the symmetry of the site, which makes it very different from the features of the states of the B cations in other two compounds. These results provide useful insights into the trends in the properties of CoB_2O_4 compounds with variation of B cation which would help in understanding the results of recent experiments on doping of Mn and Cr in multiferroic $CoCr_2O_4$.

I. INTRODUCTION

Semiconductor oxides in spinel structure have drawn considerable attention over many decades as apart from their potentials as technologically important materials¹⁻⁵ they serve as a class of materials to understand fundamental physics of magnetic interactions, electron-electron correlations and coupling of various degrees of freedom. Magnetic spinels with different magnetic cations at crystallographic inequivalent sites are interesting due to the challenges they pose in understanding the complexities that arise out of different magnetic interactions. The technological importances of magnetic spinels have been reaffirmed by the recent discovery of multiferrocity in $CoCr_2O_4$.⁶ Various collinear and non-collinear structures populate the phase diagram^{7,8} of this material as a direct consequence of interplay of magnetic exchanges, electron-electron correlation and structural distortions. In order to explore possible multi-functionalities in this multiferroic, very recently, attempts were made to study material properties by adding a third magnetic atom. The substitution of Cr by Fe resulted in new phenomena like magnetic compensation, sign reversal of Exchange Bias (EB) effect⁹⁻¹¹ at a critical temperature and significant magnetostriction¹². Recent structural and magnetic studies¹³ upon substitution of Cr by Mn in $CoCr_2O_4$ too showed a composition and temperature induced magnetisation compensation, along with a composition dependent structural transformation.

These results imply that the substitution of Cr by another magnetic atom renormalises the intra and inter-sublattice magnetic interactions and can be directly connected to the novel magnetism related phenomena. However, in order to understand the basic physics of such complex phenomena and interpret the experimental observations, one need to have a clearer understanding at the microscopic level. Such understanding can be achieved if the end compounds that is

$CoCr_2O_4$, $CoMn_2O_4$ and $CoFe_2O_4$ are investigated in a systematic manner and various physical properties of these materials are understood at a microscopic level, that is, from their electronic structures.

The standardised parameter-free approach to calculate the electronic structures and the physical properties is the various implementations of the Density Functional theory (DFT)¹⁴. There is no systematic exploration of the compounds under consideration here using DFT based electronic structure methods. There have been very few DFT based calculations of $CoCr_2O_4$ ^{15,16} and of $CoFe_2O_4$ ¹⁷⁻¹⁹ only. These calculations provided important insights into the interrelations of sub-lattice occupancies, structural properties and magnetic properties of these materials on the basis of their electronic structures.

In this communication, we present a systematic study of the three compounds CoB_2O_4 (B=Cr,Mn,Fe) with the focus on understanding the similarities and differences in their electronic structures, and thus the structural and magnetic properties in particular. We do these using DFT based calculations. Detailed information on the structural parameters, their influences on the electronic structures, the variations in the crystal fields and exchange fields and their effects on the magnetic properties as one changes the B element are provided. These results serve as important prerequisites to analyse the systems when they are doped with a third magnetic atom. The paper is organised as follows: section II details the computational tools used, section III provides and analyses the results followed by the conclusions.

II. COMPUTATIONAL DETAILS

We have used DFT+U²⁰ method for all our calculations in order to address the electron electron strong correlation effects which is necessary for oxide systems. Among various different adoptions of DFT+U, we have

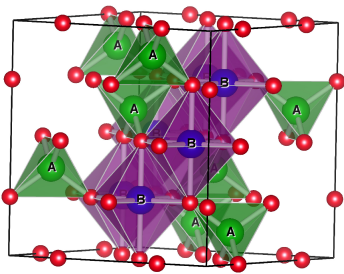


FIG. 1. The crystal structure of spinel compounds AB_2O_4 . The A , B and oxygen atoms are shaded in green, purple and red respectively.

used the approach of Dudarev *et al*²¹ where the effects of on-site Coulomb correlation and Hund's coupling are represented through an effective parameter $U_{eff} = U - J$, U being the strength of the Coulomb interaction and J the Hund's coupling. In our calculations, J has been kept at 1 eV as previous DFT calculations for a number of transition metal oxides showed that J remains nearly constant for the entire transition metal series²². The coulomb parameter U has been taken to be 3 eV for Cr, 4 eV for Mn and Fe, 5 eV for Co. The rationale behind such choices have been explained earlier¹⁶. The self-consistent quantum mechanical equations are solved using the projector augmented wave (PAW)²³ basis set as implemented in VASP code²⁴. The exchange correlation part of the Hamiltonian was treated with the PBE-GGA²⁵ functional. A plane wave cut off of 550 eV and a $5 \times 5 \times 5$ mesh centered at Γ point for Brillouin zone integrations have been used throughout to ensure an energy convergence of 10^{-7} eV. For structural relaxations the convergence criteria of force on each atom was set to be 10^{-4} eV/Å.

III. RESULTS AND DISCUSSIONS

A. Modeling of the sub-lattice occupancy and spin configuration

The spinel structure belongs to cubic space group $Fd\bar{3}m$ with two types of cation sublattice- A and B . The A sublattice has tetrahedral symmetry and is usually occupied by a cation in +2 state. The B sublattice has octahedral symmetry and is usually occupied by a cation in +3 state (Figure 1). One formula unit of spinel consists of one A sublattice and two B sublattices. In case of one B atom occupying the tetrahedral positions by displacing the A atom to the octahedral sites, the structure is known as 'Inverse Spinel'. Among the three compounds under consideration, the $CoCr_2O_4$ is found to be crystallising in 'Normal spinel' structures²⁶. In case of $CoMn_2O_4$, although the sub-lattice occupancy conforms to that of spinel, the crystal structure is tetrago-

nal with space group $I4_1/amd$ ²⁷. $CoFe_2O_4$, on the other hand, has no structural distortion, but has the sub-lattice occupancy alike Inverse spinel²⁸. The sub-lattice occupancies in $CoFe_2O_4$ is found out to be crucial in determining whether the ground state is insulator or half-metal^{17,18}. Regarding the ground state magnetic structure, Neutron diffraction studies have shown that $CoCr_2O_4$ and $CoMn_2O_4$ have canted spin structures^{27,29} while $CoFe_2O_4$ has a ferrimagnetic collinear structure, with the moments at A and B sites anti-aligning, giving rise to the Neel configuration²⁸. Mossbauer studies³⁰ later confirmed this.

The sub-lattice occupancy for $CoCr_2O_4$ and $CoMn_2O_4$ have been taken to be like normal spinels as have been found from experiments. For $CoFe_2O_4$, inverse spinel sub-lattice occupancy with maximum inversion has been considered. In absence of disorder at a particular sub-lattice, this configuration is found to be having the lowest energy¹⁸. Since modeling of the sub-lattice disorder requires either construction of a supercell in the present approach or consideration of a mean field configuration averaging procedure¹⁹, we have considered the complete inverse spinel type sub-lattice occupancy. Since the motivation behind this work is a systematic understanding of the three systems as the chemical identity of the B atom changes, we have taken the magnetic configurations of the three systems to be collinear. Although $CoCr_2O_4$ and $CoMn_2O_4$ have non-collinear magnetic ground states, the investigations into the collinear magnetic states would provide important qualitative insights. In order to find out the relative alignments of the spins at various sub-lattices, we have taken 2 formula units of the unit cell and done total energy calculations on different collinear spin configurations. We found the Neel configuration to be energetically lowest in case of $CoCr_2O_4$ and $CoFe_2O_4$. In case of $CoMn_2O_4$, we found a magnetic configuration in which the spins at the sites of a given sub-lattice are anti-parallel, giving rise to a zero magnetic moment at each sub-lattice, lowest in energy. However, the energy of the Neel configuration is higher by about only 1 meV per atom. This result indicates that the actual magnetic ground state of $CoMn_2O_4$ would be frustrated. In subsequent analysis we have considered only the Neel configuration therefore.

B. Structural parameters

The lattice parameters obtained after full structural relaxations using DFT+U for the three compounds are given in Table I. Figure 2 provides the details of various bond lengths and bond angles, thus providing a close-up view of the structures around the tetrahedral and the octahedral sites. The lattice parameters agree well with the available experimental results. $CoCr_2O_4$ stabilises in the cubic structure with almost no local distortion at the tetrahedral site as can be seen from the ideal spinel value of 109.47° for the $O - Co - O$ angle. There is slight local distortion at the octahedral

site; the $O-Cr-O$ bond angle is 84.55° , deviating from the ideal value of 90° and the $Co-O-Cr$ bond angle is 121.53° in place of ideal value of 125° . $CoMn_2O_4$, on the other hand, has a tetragonal crystal structure with $c/a = 1.16$. Subsequently various bond distances and bond angles (FIG. 1(b)) are significantly dispersed. One can now see substantial distortion associated with the tetrahedral sites as the $O-Co-O$ bond angles are $108.14^\circ \pm 4.13^\circ$. The octahedra too distorts considerably with elongation(contraction) of $Mn-O$ bonds along $z(xy)$ directions[FIG. 3(b)]. This leads to significant variations in the $O-Mn-O$ and $Mn-O-Co$ angles. The differences in the distortions in the octahedra around the B sites in $CoMn_2O_4$ in comparison to $CoCr_2O_4$ is pictorially represented in FIG. 3. In case of $CoFe_2O_4$, our calculations produce a slight departure from the perfect cubic structure, the c -axis elongated by about 0.5%. This slight loss of cubic symmetry is due to different distortions of the octahedra around Co and Fe sites. FIG. 3(c) shows that while there is slight elongations of $Co-O$ bonds along z -direction, the $Fe-O$ bonds in the same direction contracts in comparison to the same bonds in the xy planes. This gives rise to the small tetragonality. The bond angles (FIG. 2(c)) associated with the octahedral and tetrahedral sites clearly show that the distortions associated with Co atoms in the octahedral sites. The $O-Co-O$ bond angle deviates to $88.23^\circ \pm 2^\circ$ as opposed to $O-Fe-O$ bond angle of $90.24^\circ \pm 0.07^\circ$ which is quite close to ideal spinel value of 90° . Similarly, Fe_O-O-Fe_T bond angle is 124.16° , while that of Co_O-O-Fe_T bond angle is 121.53° , a larger deviation from ideal spinel value of 125° .

The energy level diagrams based upon the electronic configurations of the cations occupying the tetrahedral and octahedral sites can explain the observed trends in the structural aspects of the CoB_2O_4 compounds considered here. Figure 4 shows that in case of $CoCr_2O_4$, the higher lying e_g states of octahedral Cr^{3+} are empty while the e_g^1 configuration of Mn^{3+} in $CoMn_2O_4$ implies degeneracy associated with this level. In order to lift the degeneracy, the symmetry of the crystal structure is lowered, giving rise to the tetragonal ground state. The largeness in the tetragonal distortion can be understood from the $(t_{2g})^3(e_g)$ configuration of the Mn^{3+} ions as explained by Dunitz and Orgel³³. In case of $CoFe_2O_4$, the degeneracy associated with the t_{2g} orbitals of the Co^{2+} ions leads to the lowering of the cubic symmetry. The small value of the distortion can once again be understood from the $(t_{2g})^5(e_g)^2$ of the Co atom in the octahedral site³³.

C. Electronic Structure and Magnetic moments

The configurations of d electrons at different cation sites play the most important role in determining the electronic and magnetic properties of spinel oxides. According to crystal field theory³⁴, the electronic configuration depends on the relative strengths of the

crystal field(CF) and intra-atomic exchange field(EX). In this subsection, we attempt an understanding of the relation between the structural distortions and electronic structures in CoB_2O_4 compounds by investigating the relative strengths of crystal field splitting and exchange splitting through an analysis of the densities of states. Consequently, this would lead to the understanding of the electronic and magnetic properties of these systems.

The schematic representation of electrons in d levels in Fig. 4, based upon crystal field theory, shows that in a tetrahedral crystal field, the e_g levels lie lower than the t_{2g} levels due to direct electrostatic repulsion between the t_{2g} orbitals and the surrounding anion orbitals, while in an octahedral crystal field, the order is reversed as the e_g orbitals are repelled in this case. Upon tetragonal distortion, the e_g levels associated with the octahedral sites further split into two levels with $d_{x^2-y^2}$ orbital at a energy higher than d_{z^2} , and the t_{2g} level splits into a higher d_{xy} level and a lower doubly degenerate $d_{zy}(d_{zx})$ level when $c/a > 1$. The spacings of these energy levels depend on the strengths of the crystal fields and the exchange fields.

In Table II we present results for crystal field splitting (Δ_{CF}) and the exchange splitting (Δ_{EX}) for the three compounds. These results are obtained without incorporation of correlations that is by setting $U_{eff} = 0$. A comparison of results for the three show that the stronger exchange splitting associated with the t_{2g} states, in comparison to crystal field splitting, is a common feature for the compounds. This should lead to high spin states for both magnetic cations. The results suggest that for all three materials, the five-fold $3d$ crystal degeneracy is barely broken for the down spin(\downarrow)channel of A site. Therefore, irrespective of the chemical identity of the species at A site, this spin band is nearly full. For $CoCr_2O_4$ and $CoMn_2O_4$, the other $3d$ electrons mostly occupy the exchange split ($\Delta_{EX}^{e_g} = 1.6$ eV) e_g up spin (\uparrow) channel. In case of $CoFe_2O_4$, the exchange splitting of e_g levels is double that of the other two compounds. This is due to the fact that in $CoFe_2O_4$, the Fe^{3+} occupies the tetrahedral sites having two electrons less than Co^{2+} which occupies tetrahedral sites in the other two compounds, making the e_g^{\uparrow} states nearly empty. The t_{2g}^{\uparrow} states in all cases are energetically higher and thus remain mostly unoccupied (Not shown here), the exchange splitting associated with t_{2g} states ($\Delta_{EX}^{t_{2g}}$) being nearly constant, therefore.

The large exchange splitting of the t_{2g} states at the B site for $CoCr_2O_4$ and $CoMn_2O_4$ indicate that one of the spin bands is nearly full and the other nearly empty. This indeed is the case with the t_{2g}^{\uparrow} bands nearly full in both cases(Not shown here). For $CoFe_2O_4$, there are two different values of $\Delta_{EX}^{t_{2g}}$ corresponding to Fe^{2+} and Co^{2+} . While the exchange splitting for Fe is nearly same as that of Cr and Mn, it is smaller for Co. The reason is that Co^{2+} has two more electrons than Cr(Mn,Fe)

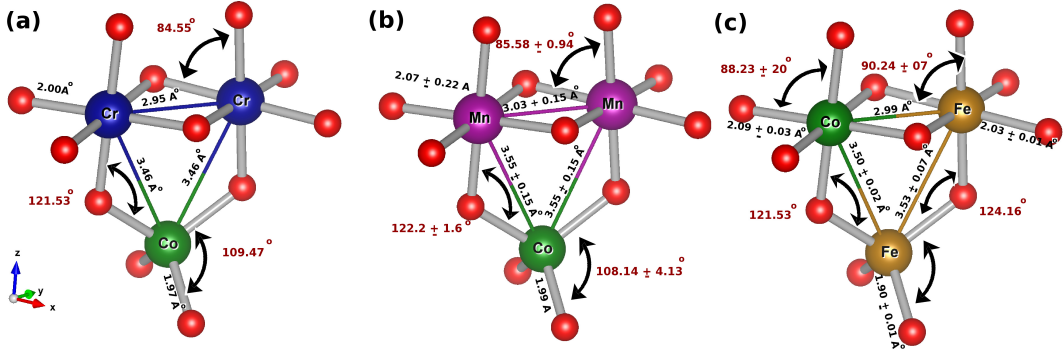


FIG. 2. The neighborhood around the tetrahedral and the octahedral sites in (a) CoCr_2O_4 , (b) CoMn_2O_4 and (c) CoFe_2O_4 along with the bond lengths and bond angles.

TABLE I. The lattice parameters of CoB_2O_4 . a, b, c are the lattice constants. x, y, z are the Oxygen parameters.

Structural parameter	CoCr_2O_4	CoMn_2O_4	CoFe_2O_4
$a(\text{\AA})$	8.35(8.34 ^a)	8.17(8.1 ^{b,c})	8.41(8.366 ^d)
$b(\text{\AA})$	8.35(8.34 ^a)	8.17(8.1 ^{b,c})	8.41(8.366 ^d)
$c(\text{\AA})$	8.35(8.34 ^a)	9.39(9.13 ^b , 9.3 ^c)	8.45(8.366 ^d)
x	0.262(0.264 ^a)	0.255(0.23 ^b)	0.255(0.256 ^d)
y	0.262(0.264 ^a)	0.255(0.23 ^b)	0.255(0.256 ^d)
z	0.262(0.264 ^a)	0.267(0.256 ^b)	0.255(0.256 ^d)

a : Reference³¹ b : Reference²⁷ c : Reference³² d : Reference²⁸

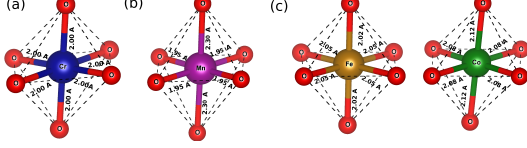


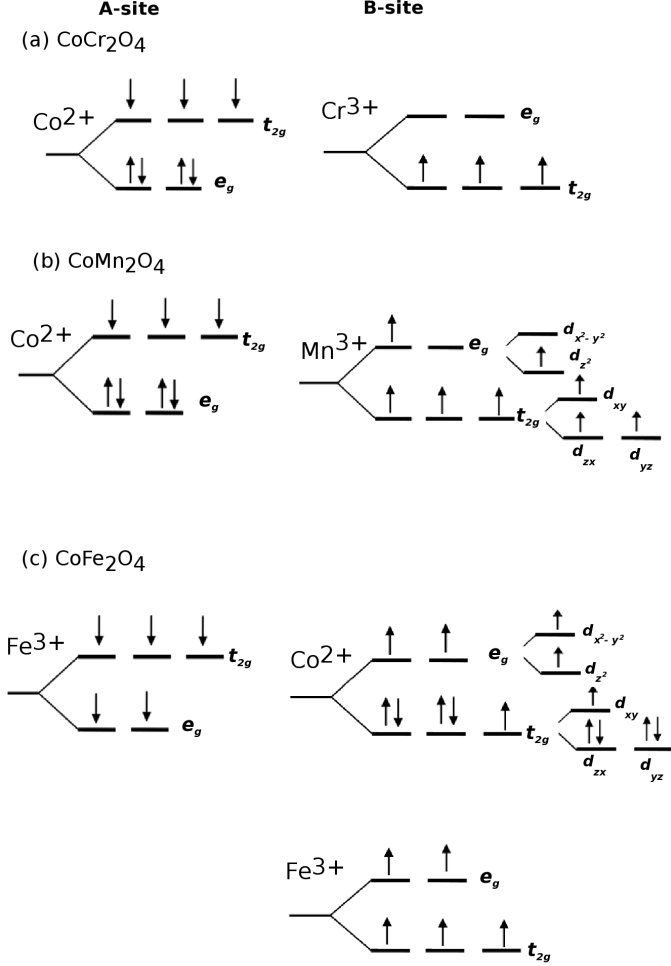
FIG. 3. The neighbourhood around the octahedral site of (a) CoCr_2O_4 , (b) CoMn_2O_4 and (c) CoFe_2O_4 providing a close up view of the distortions associated with the octahedra.

and hence part of the down (\downarrow) spin channel is also occupied. The exchange splitting of e_g states at the B site for CoCr_2O_4 and CoMn_2O_4 are much smaller as the e_g band is nearly empty for both spins. One extra electron in the e_g band of CoMn_2O_4 in comparison to CoCr_2O_4 increases $\Delta_{EX}^{e_g}$ for the former. In case of CoFe_2O_4 , $\Delta_{EX}^{e_g}$ are comparable for both Co and Fe at the B site. This is expected as both Co^{2+} and Fe^{3+} have one spin channel completely full and the other completely empty. The extra electron in Mn^{3+} e_g band (as compared to Cr^{3+}) explains the reason behind smaller values of crystal field splitting (for both bands) in CoMn_2O_4 than in CoCr_2O_4 . In CoFe_2O_4 , Δ_{CF}^\downarrow for both Co^{2+} and Fe^{3+} are the largest while Δ_{CF}^\uparrow are smaller than that for Cr^{3+} and Mn^{3+} in the other two compounds. The smaller values of Δ_{CF}^\uparrow are due to the fact that for both cations, up (\uparrow) bands

are nearly full and therefore, the centers of t_{2g}^\uparrow and e_g^\uparrow bands lie much closer than those of Cr^{3+} and Mn^{3+} in the other two compounds. The largest crystal field splittings for up (\uparrow) bands of Co^{2+} and Fe^{3+} in CoFe_2O_4 are due to the facts that unlike Cr^{3+} and Mn^{3+} in other two compounds, the t_{2g}^\downarrow are not completely empty. Thus, the separation between t_{2g}^\downarrow and e_g^\downarrow are larger compared to the other two. The outcome of the competition between the crystal field splitting and the exchange splitting would affect the semiconducting band gap in these materials. In case of CoCr_2O_4 , equally strong exchange splitting and crystal field splitting at Cr site decides the gap. For the other two compounds, weaker crystal field splitting compared to the exchange splitting at B sites should result in decrease in the band gap as the B occupation changes from Cr to Mn and Fe. However, with the GGA only calculations, ground states of CoMn_2O_4 and CoFe_2O_4 are metallic. This is because of the presence of finite densities of t_{2g} states at the Fermi level of B site atoms (Not shown here). This can be correlated to the fact that without the inclusion of strong correlations, CoMn_2O_4 crystallizes in cubic structure, thus unable to obtain the symmetry breaking of the d orbitals and distribution of states on both sides of the Fermi level. In case of CoFe_2O_4 , the distortion at the Co site is small and thus the local symmetry is barely broken, resulting in the localisation of states at the Fermi level. The inclusion of electron-electron correlation through GGA+U

TABLE II. Exchange Splitting (Δ_{EX}) and crystal field splitting (Δ_{CF}) results for the three compounds.

System	ion	At tetrahedral site				ion	At Octahedral site			
		$\Delta_{EX}^{e_g}$	$\Delta_{EX}^{t_{2g}}$	Δ_{CF}^{\downarrow}	Δ_{CF}^{\uparrow}		$\Delta_{EX}^{e_g}$	$\Delta_{EX}^{t_{2g}}$	Δ_{CF}^{\downarrow}	Δ_{CF}^{\uparrow}
$CoCr_2O_4$	Co^{2+}	1.6	2.9	0.0	1.3	Cr^{3+}	1.3	3.2	1.3	3.3
$CoMn_2O_4$	Co^{2+}	1.6	2.5	0.5	1.3	Mn^{3+}	1.8	3.7	0.3	2.2
$CoFe_2O_4$	Fe^{3+}	3.3	3.1	1.0	0.8	Fe^{3+}	3.5	3.7	1.7	1.9
						Co^{2+}	3.1	2.4	1.9	1.2

FIG. 4. Electronic configurations for cations occupying A and B sites in CoB_2O_4 compounds

formalism produces the correct semiconducting ground states by introducing appropriate localisation of states, and the correct crystal structures by breaking the degeneracies in the e_g orbitals of Mn cations in $CoMn_2O_4$. The total and atom projected densities of states calculated with GGA+U are presented in Figures 5, 6 and 7. In $CoCr_2O_4$, Co t_{2g}^{\downarrow} electrons are localised around -6 eV and e_g^{\downarrow} states are localised around -2 eV. In the down spin (\downarrow) band, it is the e_g states that primarily hybridise with

TABLE III. The magnetic moments of $A(\mu_A)$, $B(\mu_B)$ cations and the total moment (μ_T) per formula unit in Bohr Magneton

System	A site	μ_A	B site	μ_B	μ_T
$CoCr_2O_4$	Co	-2.66	Cr	2.94	2.95
$MnCr_2O_4$	Co	-2.68	Mn	3.81	4.84
$CoFe_2O_4$	Fe_T	-3.98	Fe_O	4.10	2.98
			Co_O	2.66	

the oxygen p states. The t_{2g}^{\uparrow} Co states are unoccupied and centred around 2-4 eV, while the 2 e_g electrons are localised between -1 eV and -2 eV in the up(\uparrow) spin channel. This gives rise to a magnetic moment of about $3 \mu_B$ at the Co site (Table III). At the Cr site, the incorporation of strong correlation does not have a very significant effect on the t_{2g} states, the t_{2g}^{\uparrow} states are still fully occupied with the electrons localised near the Fermi level while the fully unoccupied t_{2g}^{\downarrow} states are pushed towards higher energies. The t_{2g} states thus weakly hybridise with the oxygen states. The e_g band is nearly empty as it was when calculations were done without incorporating U_{eff} . This results in a magnetic moment of nearly $3 \mu_B$ for Cr atoms as well, with the sign of the moment opposite to that of Co atoms (Table III).

In $CoMn_2O_4$ (Fig. 6), the t_{2g} states of Co are qualitatively similar to those in $CoCr_2O_4$, except that they are shifted as a whole towards lower energy. The e_g states at Co site are more delocalised in comparison to those in $CoCr_2O_4$ leading to more hybridisation between Co e_g^{\downarrow} and oxygen p states. This, however, still gives rise to a magnetic moment of about $3 \mu_B$ at Co site, like $CoCr_2O_4$. The densities of states at the Mn site is more interesting as the degeneracy of the d states are lifted due to large tetragonal distortion. According to crystal field theory, the higher energy e_g^{\uparrow} states should split into d_{z^2} and $d_{x^2-y^2}$ states with d_{z^2} being occupied and $d_{x^2-y^2}$ participating in covalent bond formation with oxygen³⁵. In Figure 6(bottom panel), we indeed see this happening. The half-filled $d_{z^2}^{\uparrow}$ gives rise to distinct peaks at around -6 eV and at around 1 eV. The $d_{x^2-y^2}$ states are more delocalised, having participated in hybridisations with oxygen p states. The down (\downarrow) spin channel is nearly empty, leading to a Mn moment of nearly $4 \mu_B$ (Table III). The lifting of degeneracy has less effect on the t_{2g} states except that they are more delocalised in

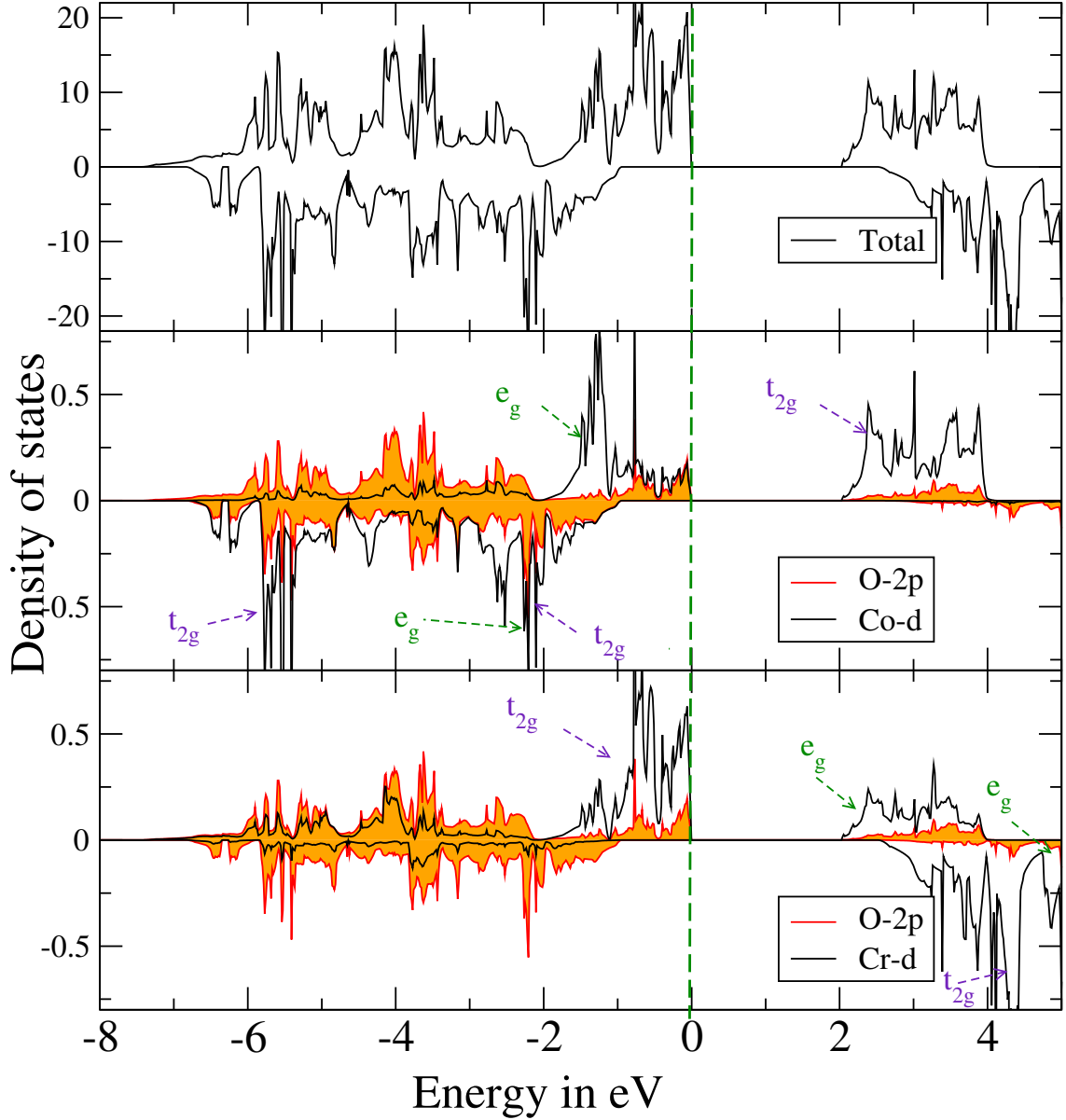


FIG. 5. The total(top panel) and site projected densities of states(A site in the middle panel and B site in the bottom panel, along with the the anion contributions) for $CoCr_2O_4$. The energies are plotted with respect to Fermi level.

comparison to the case when effect of electron electron correlation was absent and the crystal structure was cubic. Overall, the extra electron in the e_g band of Mn (in comparison to Cr) gives rise to states closer to the Fermi level and thus reduces the electronic band gap in $CoMn_2O_4$ in comparison to the band gap in $CoCr_2O_4$ as expected. The calculated band gap in $CoCr_2O_4$ is 2.1 eV while that of $CoMn_2O_4$ is 0.33 eV.

In $CoFe_2O_4$, different sub-lattice occupancy due to the 'Inverted' structure introduces qualitative differences of both A and B sites densities of states (Fig. 7). The introduction of strong correlations pushes the unoccupied states in the spin up band towards higher energy. The completely filled spin down band has electrons extremely

localised around -6 eV to -7 eV allowing little hybridisations with the oxygen states. This leads to a moment of $4 \mu_B$ for Fe_T atoms. At the octahedral site, there are two types of atoms, Fe_O and Co. We see qualitatively very different features of the states associated with these two atoms. The e_g^\downarrow band is completely empty for either atoms. For Fe_O , the t_{2g}^\uparrow band is completely full and is extremely localised around -6 eV to -7 eV. Thus, irrespective of the crystal environment, Fe states are localised in $CoFe_2O_4$. The Co states in the octahedral sites are, however, delocalised, particularly in the spin up band. The distortions associated with the Co site, breaks the t_{2g} degeneracy only slightly. In the down spin band, the d_{zx}, d_{yx} states give rise to states near Fermi level (peaks close to -1 eV).

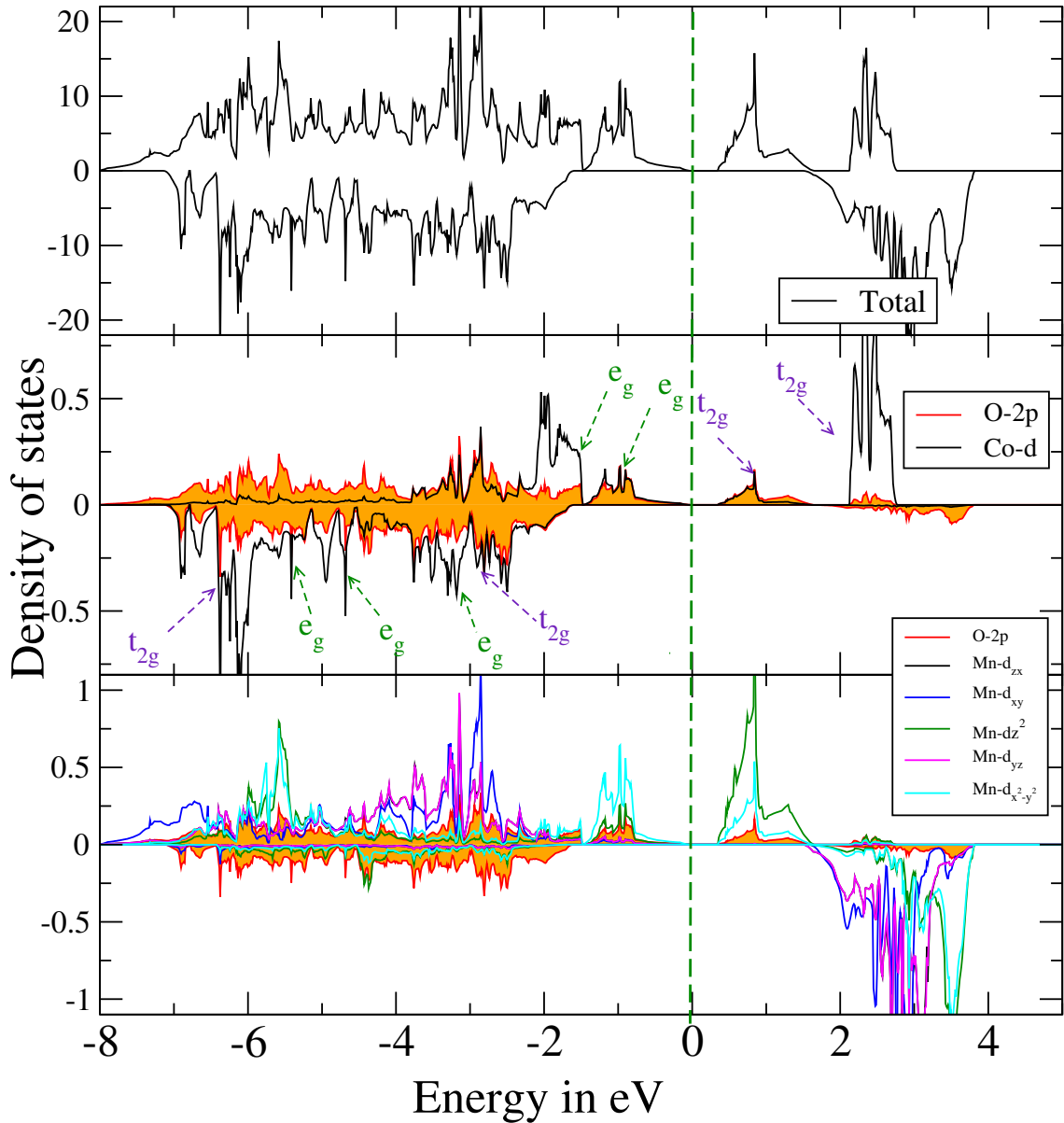


FIG. 6. The total(top panel) and site projected densities of states(A in the middle and B in the bottom panel along with anion contributions) for $CoMn_2O_4$. The Energies are plotted with respect to Fermi level.

There were no such states associated with the octahedral sites in the other two compounds. The extra electrons in Co, in comparison to Cr and Mn, are responsible for these states. This, in turn, reduces the band gap, in comparison to $CoCr_2O_4$; the calculated band gap of $CoFe_2O_4$ being 1.14 eV. The t_{2g}^{\uparrow} states of Co are delocalised, hybridising with the oxygen p states. The magnetic moments are, therefore about $3 \mu_B$ and $4 \mu_B$ for Co and Fe_O in $CoFe_2O_4$ (Table III).

The comparative study of the electronic structure, thus, shows that the Co states are delocalised irrespective of the crystal environment while the Fe states are extremely localised in CoB_2O_4 compounds considered. This would have important consequences on the mag-

netic exchange interactions and therefore the spin structures of the pristine compounds as well as in doped systems which have been investigated experimentally only recently^{9,12,13}. In the next subsection we compute and discuss the magnetic exchange interactions of these compounds.

D. Magnetic Exchange Interactions

The magnetic exchange interactions are computed by mapping the GGA+U total energies of different collinear spin configurations on to a Heisenberg Hamiltonian¹⁶. The results for the nearest neighbour interactions are

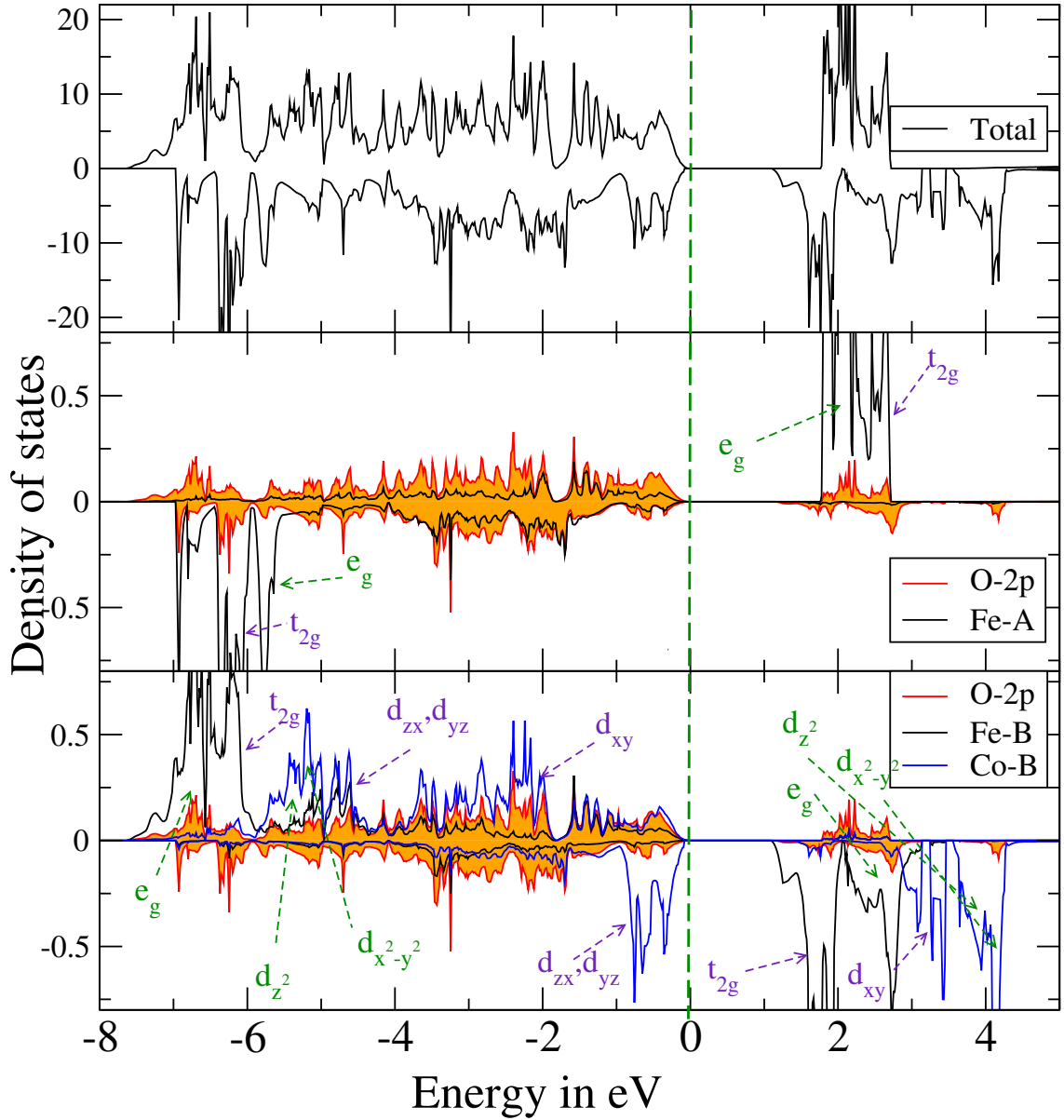


FIG. 7. The total(top panel) and site projected densities of states(A in the middle panel and B in the bottom panel along with anion contributions) for $CoFe_2O_4$. The energies are plotted with respect to Fermi level.

presented in Table IV. The higher neighbour exchange interactions are smaller by an order of magnitude and hence they are not considered for discussions. The results show that the A-A interactions are the weakest and therefore, is not expected to play any significant role. This is consistent with the discussion by Kaplan³⁶. In $CoCr_2O_4$, the A-B and B-B exchange interactions are comparable. In this case B site t_{2g} orbitals are half-filled. So direct B-B interactions are possible, apart from the super-exchange via oxygen atoms. Moreover, nearly empty e_g orbitals reduce the anion shielding as partial covalency via e_g orbitals are possible. However, since the A site t_{2g} orbitals are half-filled and the B site e_g orbitals are nearly empty as seen from the densities of

states, the A-B interactions cease to be the strongest. Therefore, the A-B and B-B interactions are comparable for $CoCr_2O_4$. Due to these two interactions being comparable, the spin structure of $CoCr_2O_4$ is not collinear³⁷ as has been observed in the experiments. The calculation of the so called LKDM parameter³⁸ which characterises the magnetic structure of cubic spinels also confirmed this picture¹⁶. In $CoMn_2O_4$, the A-site t_{2g} orbitals are half-filled while the B-site e_g orbitals are less than half-filled and degenerate. This should lead to a strong antiferromagnetic A-B interaction which indeed is observed in our calculations ($J_{Co-Mn} = -3.48$ meV). As for the B-B interaction, the B-site t_{2g} orbitals are half-filled and so direct B-B interactions, apart from super-exchange via oxy-

TABLE IV. The magnetic exchange parameters (J_{ij} in meV) and the Ferrimagnetic transition temperatures(T_c in K)of the three compounds

System	Type of AA pair	J_{AA}	Type of BB pair	J_{BB}	Type of AB pair	J_{AB}	T_c
$CoCr_2O_4$	Co-Co	-0.56	Cr-Cr	-3.01	Co-Cr	-3.26	144(97 ^a)
$CoMn_2O_4$	Co-Co	-0.29	Mn-Mn	-1.05(out of plane) -9.46(in plane)	Co-Mn	-3.53	153(85 ^b)
$CoFe_2O_4$	$Fe_O - Fe_O$	-2.06	$Co_O - Co_O$ $Fe_O - Fe_O$ $Fe_O - Co_O$	0.08 -4.77 0.84	$Fe_T - Co_O$ $Fe_T - Fe_O$	-10.43 -21.65	1079(860 ^c)

a: Reference³¹ *b*: Reference³² *c*: Reference²⁸

gen is possible. However, the strength of this interaction would depend on the inter-cation distance³⁵. Due to the tetragonal distortion, the in-plane Mn-Mn distances are short ($\sim 2.88\text{\AA}$) and thus the direct interactions are extremely strong ~ -9.5 meV (Table IV). The out-of-plane Mn-Mn distances are, on the other hand are $\sim 3.11\text{\AA}$. This weakens the B-B interactions and are only ~ -1.05 meV. This huge anisotropy in the exchange interactions due to the tetragonal distortion leads to a complicated non-collinear spin structure²⁷. This anisotropy in the $CoMn_2O_4$ was discussed earlier³⁹ but was never calculated from first-principles. Our calculations provided the quantitative credence to the original idea.

In case of $CoFe_2O_4$, the overwhelmingly dominant interactions are the A-B interactions as is seen from our calculations. This explains the reason behind a collinear spin structure of this system. The reason behind this strong antiferromagnetic A-B interaction is that the A site t_{2g} orbitals and B site e_g orbitals (for both Fe and Co at B site) are half-filled. The reason behind a weak Co-Co and Co-Fe interactions at the B site is that the Co t_{2g} orbitals are more than half-filled and degenerate and hence no direct B-B interactions occurs between them. Fe_O-Fe_O interactions are stronger than these two as the t_{2g} orbitals of Fe_O are half-filled and hence direct interactions are possible. However, since the Fe_O e_g orbitals are also half-filled, partial covalency with anions is also not possible(as seen in the extremely localised Fe densities of states), leading to a large anion shielding and a subsequent reduction in the B-B interaction in comparison to the A-B interaction.

The ferrimagnetic transition temperatures (T_C) are calculated using these exchange interactions and under mean field approximation, as done in Ref.¹⁶. Our calculated results and a comparison with experimental values are presented in Table IV. As expected, the critical temperatures calculated by a Mean field approximation overestimates the values. However, the calculated values reproduce the trends seen in the experiments with $CoFe_2O_4$ having a large T_C due to very large values of J_{AB} while the other two have rather small values of T_C due to competing J_{AB} and J_{BB} leading to non-collinear magnetic structures.

IV. CONCLUSIONS

We have performed a systematic investigations into the structural and magnetic properties of CoB_2O_4 magnetic spinels by changing the B cation using first-principles Density functional theory based methods. The understanding of the properties of these compounds is done by quantifying the relative strengths of the crystal field effect and the exchange effect through an analysis of their electronic structures. We find that the electron-electron interactions of the magnetic cations play a very important role and without the incorporation of this, the correct ground state structures cannot be obtained. The strong electron correlations are responsible for significant local structural distortions at the octahedral site and global tetragonal distortions for $CoMn_2O_4$. These are responsible for the trends in the electronic properties such as the band gap. The electronic structures of these compounds are significantly different as the B site cation is changed. This, in turn, affects the inter-atomic magnetic exchange interactions considerably and is responsible for very different spin structures of these systems. In this work, for the first time, understanding of the trends in the magnetic properties are attempted through proper quantification of the associated quantities and by providing necessary explanations from the trends in the local structural parameters and the electronic structures. The results hold immense significance with regard to the recent experimental results on $Co(Cr_{1-x}Fe_x)_2O_4$ and $Co(Cr_{1-x}Mn_x)_2O_4$ systems, where the chemical properties of the third magnetic atom in $CoCr_2O_4$, the sublattice occupancies and the structural distortions are thought to be giving rise to interesting functional properties. In future communications, these issues will be addressed.

V. ACKNOWLEDGMENTS

The computation facilities from C-DAC, Pune, India and from Department of Physics, IIT Guwahati funded under the FIST programme of DST, India are acknowledged.

-
- ¹ N.V.Kuleshov, V.P.Mikhailov, and V.G.Scherbitsky, *Proc. SPIE*, **175**, 2138 (1994)
 - ² A.Jouini, A.Yoshikawa, A.Guyot, A.Breiner, T.Fukuda, and G.Boulon, *Opt. Mater.* **30**, 47 (2007)
 - ³ K.G. Tshabalala, S.H.Cho, J.K.Park, S.S.Pitale, I.M.Nagpure, R.E.Kroon, H.C.Swart, and O.M.Ntwaeaborwa *J. Alloys. Compds.* **509**, 10115 (2011)
 - ⁴ Y.X.Li, P.J.Niu, L.Hu, X.W.Xu, and C.C.Tang *J. Lumin.* **129**, 1204 (2009)
 - ⁵ P.J.Deren, K.Maleszka-Baginska, P.Gluchowski, and M.A.Malecka *J.Alloys.Compds.* **525**, 39 (2012)
 - ⁶ Y.Yamasaki, S.Miyasaka, Y.Kaneko, J.-P.He, T.Arima and Y. Torakuma, *Phys. Rev. Lett.* **96**, 207204 (2006)
 - ⁷ K.Tomiyasu, J.Fukunaga and H.Suzuki, *Phys. Rev. B* **70**, 214434 (2004)
 - ⁸ L.J.Chang, D.J.Huang, W.-H Li, S.-W. Cheong, W. Ratcliff and J.W.Lyn, *J.Phys.Condens. Matt.* **21**, 456008 (2009)
 - ⁹ R.Padam, S.Pandya, S.Ravi, A.K.Nigam, S.Ramakrishnan, A.K.Grover and D.Pal, *Appl. Phys. Lett.* **102**, 112412 (2013)
 - ¹⁰ R.Padam, S.Pandya, S.Ravi, A.K.Nigam, S.Ramakrishnan, A.K.Grover and D.Pal, *AIP Conference Proceedings* **1512**, 1112 (2013)
 - ¹¹ R.Padam, Ph.D.Thesis, IIT Guwahati (2014)
 - ¹² H.-Zhang, W.-Wang, En-Liu, X.-Tang, G.-Li, H.-Zhang and G.-Wu, *Phys. Stat. Solidi B* **250**, 1287 (2013)
 - ¹³ H.G.Zhang, Z.Wang, E.K.Liu, W.H.Wang, M.Yue and G.H.Wu, *J. Appl. Phys.* **117**, 17B735 (2015)
 - ¹⁴ P. Hohenberg and W. Kohn, *Phys. Rev.* **B136**, 864 (1964); W.Kohn and L.J.Sham, *Phys. Rev.* **A140**, 1133 (1965)
 - ¹⁵ C.Ederer and M. Komelj, *Phys. Rev.* **B76**, 064409 (2006)
 - ¹⁶ D.Das and S. Ghosh, *J. Phys. D:Appl. Phys.* **48**, 425001 (2015)
 - ¹⁷ D.Fritsch and C.Ederer, *Phys. Rev.* **B82**, 104117 (2010)
 - ¹⁸ Y.H.Hou, Y.J.Zhao, Z.W.Liu, H.Y.Yu, X.C.Zhong, W.Q.Qiu, D.C.Zeng and L.S.Wen, *J.Phys.D: Appl. Phys.* **43**, 445003 (2010)
 - ¹⁹ S.Ganguly, R.Chimata and B.Sanyal, *Phys. Rev.* **B92**, 224417 (2015)
 - ²⁰ V.I.Anisimov, F.Aryasetiawan and A.I. Liechtenstein, *J. Phys. Condens. Matt.* **9**, 767 (1997)
 - ²¹ S.L.Dudarev, G.A.Botton, S.Y.Savrasov, C.J.Humphreys and A.P.Sutton, *Phys. Rev.* **B57**, 1505 (1998)
 - ²² I.Solovyev, N.Hamada and K.Terakura, *Phys. Rev.* **B53**, 7158 (1996)
 - ²³ P.E.Bloch, *Phys. Rev.* **B50**, 17953 (1994)
 - ²⁴ G.Kresse and J. Furthmuller, *Comput. Mater. Sci.* **6**, 15 (1996)
 - ²⁵ J. P. Perdew, K. Burke, and M. Ernzerhof, *Phys. Rev. Lett.* **77**, 3865 (1996)
 - ²⁶ N.Menyuk, K.Dwight and A.Wold, *J. Phys.(Paris)* **25**, 528 (1964)
 - ²⁷ B. Boucher, R. Buhl and M. Perrin, *J. Appl. Phys.* **39**, 632 (1968)
 - ²⁸ J. Teillet F. Bouree and R. Krishnan *J. Magn. Magn. Mater.* **123**, 93-96 (1993)
 - ²⁹ K. Tomiyasu, J. Fukunaga, and H. Suzuki, *Phys. Rev.* **B70**, 214434 (2004)
 - ³⁰ S.J.Kim, S.W.Lee and C.S.Kim, *Jpn. J. Appl. Phys.*, **40**, 4897 (2001)
 - ³¹ G. Lawes, B.Melot, K.Page, C.Ederer, M.A.Hayward, T.Proffen and R. Seshadri, *Phys. Rev.* **B74**, 024413 (2006)
 - ³² D.G.Wickham and W.J.Croft, *J. Phys. Chem. Solids.* **7**, 351 (1958)
 - ³³ J.D.Dunitz and L.E.Orgel, *J. Phys. Chem. Solids* **3**, 20 (1957)
 - ³⁴ I.B.Berusker, *Electronic structure and Properties of Transition Metal Compounds: Introduction to the Theory* (New York: Wiley) (1996)
 - ³⁵ D.G.Wickham and J.B.Goodenough, *Phys. Rev.* **115**, 1156 (1959)
 - ³⁶ T.A.Kaplan, *Phys. Rev.*, **119**, 1460 (1960)
 - ³⁷ Y.Yafet and C.Kittel, *Phys. Rev.*, **87**, 290 (1952)
 - ³⁸ D.H.Lyons, T.A.Kaplan, K.Dwight and N. Menyuk, *Phys. Rev.* **126**, 540 (1962)
 - ³⁹ J.B.Goodenough, *Magnetism and the Chemical Bond* (John Wiley) (1963)